Narrowing of the neutron sd-pf shell gap in 29Na: First in-beam gamma-ray spectroscopy results using TIGRESS at ISAC-II

A. M. Hurst, C. Y. Wu, J. A. Becker, M. A. Stoyer, C. J. Pearson, G. Hackman, M. A. Schumaker, C. E. Svenson, R. A. Austin, G. C. Ball, D. Bandyopadhyay, C. J. Barton, A. J. Boston, H. C. Boston, R. Churchman, D. Cline, S. J. Colosimo, D. S. Cross, G. Demand, M. Djongolov, T. E. Drake, P. E. Garrett, C. Gray-Jones, K. L. Green, A. N. Grint, A. B. Hayes, K. G. Leach, W. D. Kulp, G. Lee, S. Lloyd, R. Maharaj, J. Martin, B. A. Millar, S. Mythili, L. Nelson, P. J. Nolan, D. C. Oxley, E. Padilla-Rodal, A. A. Phillips, M. Porter-Peden, S. V. Rigby, F. Sarazin, C. S. Sumithrarachchi, S. Triambak, P. M. Walker, S. J. Williams, J. Wong, J. L. Wood

January 28, 2009

Disclaimer

This document was prepared as an account of work sponsored by an agency of the United States government. Neither the United States government nor Lawrence Livermore National Security, LLC, nor any of their employees makes any warranty, expressed or implied, or assumes any legal liability or responsibility for the accuracy, completeness, or usefulness of any information, apparatus, product, or process disclosed, or represents that its use would not infringe privately owned rights. Reference herein to any specific commercial product, process, or service by trade name, trademark, manufacturer, or otherwise does not necessarily constitute or imply its endorsement, recommendation, or favoring by the United States government or Lawrence Livermore National Security, LLC. The views and opinions of authors expressed herein do not necessarily state or reflect those of the United States government or Lawrence Livermore National Security, LLC, and shall not be used for advertising or product endorsement purposes.

Narrowing of the neutron sd-pf shell gap in ^{29}Na: First in-beam γ-ray spectroscopy results using TIGRESS at ISAC-II[*]

A. M. Hurst,[1,†] C. Y. Wu,[1] J. A. Becker,[1] M. A. Stoyer,[1] C. J. Pearson,[2] G. Hackman,[2] M. A. Schumaker,[3]
C. E. Svensson,[3] R. A. E. Austin,[4] G. C. Ball,[2] D. Bandyopadhyay,[2] C. J. Barton,[5] A. J. Boston,[6]
H. C. Boston,[6] R. Churchman,[2] D. Cline,[7] S. J. Colosimo,[4] D. S. Cross,[8] G. Demand,[3] M. Djongolov,[2]
T. E. Drake,[9] P. E. Garrett,[3] C. Gray-Jones,[6] K. L. Green,[3] A. N. Grint,[6] A. B. Hayes,[7] K. G. Leach,[3]
W. D. Kulp,[10] G. Lee,[2] S. Lloyd,[2] R. Maharaj,[2] J-P. Martin,[11] B. A. Millar,[3] S. Mythili,[12] L. Nelson,[6]
P. J. Nolan,[6] D. C. Oxley,[6] E. Padilla-Rodal,[2] A. A. Phillips,[3] M. Porter-Peden,[13] S. V. Rigby,[6] F. Sarazin,[13]
C. S. Sumithrarachchi,[3] S. Triambak,[3] P. M. Walker,[14] S. J. Williams,[2] J. Wong,[3] and J. L. Wood[10]

[1]*Lawrence Livermore National Laboratory, Livermore, California 94550, USA*
[2]*TRIUMF, 4004 Westbrook Mall, Vancouver BC, V6T 2A3, Canada*
[3]*Department of Physics, University of Guelph, Guelph ON, N1G 2W1, Canada*
[4]*Department of Astronomy and Physics, Saint Mary's University, Halifax NS, B3H 3C3, Canada*
[5]*Department of Physics, University of York, York YO10 5DD, United Kingdom*
[6]*Oliver Lodge Laboratory, University of Liverpool, Liverpool L69 7ZE, United Kingdom*
[7]*Department of Physics and Astronomy, University of Rochester, Rochester, NY 14627, USA*
[8]*Department of Chemistry, Simon Fraser University, Burnaby BC, V5A 1S6, Canada*
[9]*Department of Physics, University of Toronto, Toronto ON, M5S 1A7, Canada*
[10]*School of Physics, Georgia Institute of Technology, Atlanta, Georgia 30332, USA*
[11]*Department of Physics, University of Montreal, Montreal QC, G1K 7P4, Canada*
[12]*Department of Physics, University of British Columbia, Vancouver BC, V6T 1Z1, Canada*
[13]*Physics Department, Colorado School of Mines, Golden, Colorado 80401, USA*
[14]*Deptartment of Physics, University of Surrey, Guildford, Surrey GU2 7XH, United Kingdom*
(Dated: January 27, 2009)

In the first in-beam γ-ray spectroscopy experiment using TIGRESS at the recently commissioned ISAC-II facility at TRIUMF, the wave-function composition for the low-lying states in ^{29}Na was explored by measuring their electromagnetic properties using the Coulomb-excitation technique. A beam of ^{29}Na ions, postaccelerated to $2.41 \cdot A$ MeV, bombarded a ^{110}Pd target with a rate of up to 600 particles per second. The TIGRESS γ-ray spectrometer, comprising six 32-fold segmented HPGe clover detectors, was used to record deexcitation γ rays in coincidence with scattered or recoiling charged particles detected in a silicon detector, BAMBINO, which is segmented in both the polar and azimuthal planes. A value for the reduced transition matrix element $|\langle \frac{5}{2}^+_1 || E2 || \frac{3}{2}^+_{\text{gs}} \rangle| = 0.237(21)$ eb was derived for ^{29}Na from the measured γ-ray yields for both projectile and target. A comparison of this experimental result with the most recent large-scale Monte Carlo shell-model calculation suggests a significant admixture of both sd and pf components in the wave function. Furthermore, this result implies a narrow sd-pf neutron-shell gap of only ~ 3 MeV for ^{29}Na, rather than ~ 6 MeV for nuclei in the vicinity of the valley of β stability.

PACS numbers: 21.10.Ky, 23.40.Hc, 25.70.De, 27.30.+t

I. INTRODUCTION

Since the first observation of the neutron-rich Na isotopes in the region of the $N = 20$ semi-magic shell closure, identified by Kalpisch *et al.* in high-energy nuclear reactions [1], their intriguing properties remain the subject of much ongoing experimental and theoretical debate. Direct mass measurements by Thibault *et al.* later revealed the ^{31,32}Na isotopes to be more tightly bound than expected [2] according to conventional shell-model ordering. A proposed explanation for this surprising result, supported by Hartree-Fock calculations using a Skyrme effective interaction, suggested that the Na isotopes in this mass region have a strong prolate deformation due to an inverted filling of negative parity $\nu f_{7/2}$ orbitals [3], rather than the expected $\nu d_{3/2}$ orbitals of the sd shell. It was further revealed through high-resolution laser spectroscopy [4] that the ground-state spins, magnetic moments, and charge radii of the neutron-rich $^{28-31}$Na isotopes were found to be consistent with a prolate deformation rather than a near-spherical configuration. Corresponding mass measurements of the neutron-rich Mg isotopes later showed both ^{31,32}Mg to have anomalously large binding energies [5]. In addition, the remarkably low energy of 885 keV for the first 2^+ state in ^{32}Mg [6] was a clear signature of deviation from magicity at $N = 20$.

Theoretical studies into the binding energies of $Z \approx 10 - 12$, $N \approx 20$ nuclei, demonstrated that such proper-

ties could not be understood on the basis of an interaction with the active orbits constrained to the sd shell-model space alone [7]. However, an expanded model space including the lower orbits of the pf shell allowing for neutron excitations across the sd-pf shell gap was successful in reproducing the observed trend in binding energies for the neutron-rich Na and Mg isotopes [8] in a region far from stability, known as the *island of inversion* [9], where intruder pf configurations dominate the ground-state wave function. With a general consensus that nuclei residing in this region of deformation experience enhanced binding energies due to particle-hole excitations across the sd-pf shell gap, an investigation by Warburton, Becker, and Brown [10] was undertaken in order to delineate the boundaries of this region. In their work they cite the strong $T = 0$ NN interaction [11] as the principal cause of enhanced deformation, with the narrowing of the $\nu(sd$-$pf)$ energy gap due to neutron excess an additional factor. Although their shell-model calculations utilized the full sd-pf model space, the normal (sd) and intruder (pf) spaces were diagonalised separately and they found this region limited to nine nuclei only: $^{30-32}$Ne, $^{31-33}$Na, and $^{32-34}$Mg. However, Monte Carlo shell model (MCSM) calculations based on the quantum Monte Carlo diagonalisation method [12] have since suggested that the boundaries to the island may be more complex than originally proposed in Ref. [10] when taking into account the variable mixing between normal 0p0h and intruder 2p2h configurations. Indeed experimental information regarding the electromagnetic properties of low-lying states in nuclei beyond the boundaries in Ref. [10] has also emerged in recent years confirming the role of intruder configurations at low spin, for example, in ^{28}Ne [13], ^{30}Na [14] and ^{31}Mg [15].

The key question therefore arises as to where in a given isotopic chain does the transition to the island of inversion occur. Compelling evidence suggests that the $N = 18$ nucleus ^{30}Mg is well described within the sd framework [16], while ground-state properties of neighboring $N = 19$ nucleus ^{31}Mg support a nearly-pure 2p2h intruder configuration [15]. The situation regarding the $Z = 11$ Na isotopic chain is somewhat more complicated. The low $B(E2)$ value [14] and small quadrupole moment [14, 17] of ^{28}Na can be well understood negating any cross-shell influence from the pf shell. Conversely the large $B(E2)$ value and quadrupole moment of ^{31}Na is consistent with a pf-intruder dominated ground state, while cross-shell mixing cannot be ruled out in ^{30}Na [14]. Recent studies through β^--decay spectroscopy have unraveled the level schemes of ^{28}Na and ^{29}Na up to ~ 3.5 and ~ 4.2 MeV, respectively [18, 19]. Comparison of the observed level schemes and β^- branching ratios with shell-model calculations demonstrate the influence of intruder configurations at low energy in ^{29}Na (although this interpretation is complicated by a possible 2p-2h intruder component in the ground state of ^{29}Ne [20]) but not in ^{28}Na. Furthermore, the large ground-state quadrupole moment of ^{29}Na [17] can only be explained

FIG. 1: Arrangement of the HPGe clovers of the TIGRESS array around the target chamber at the end of the ISAC-II beam line at TRIUMF. In this experiment the array comprised six 32-fold segmented clovers. The ^{110}Pd-target foil and Si-based BAMBINO are mounted inside the chamber.

by considering ~ 42 % mixing from intruder configurations in the ground state [21]. This intriguing scenario may be explained by assuming that the last few valence neutrons do not fill the expected orbitals in accordance with standard shell-model ordering near stability, but rather jump to the lower orbitals of the next major pf shell [21] and it has thus been suggested that ^{29}Na is the transition point nucleus to the island of inversion in the Na isotopic chain [18]. Such a phenomenon implies that the sd-pf shell gap narrows in ^{29}Na to an extent that the energetics are beginning to favour population of the pf shell, even though the $N = 20$ shell closure is not complete. Complex shell-model calculations performed using effective Hamiltonians incorporating the sd and pf shell-model spaces, including the cross-shell mixing terms, support this hypothesis [12, 21, 22]. The most recent calculation of ^{29}Na utilising MCSM techniques with an SDPF-M Hamiltonian [21], based on a valence shell comprising all the sd-shell orbits and the two lower orbits of the pf shell and with the effective charges $(e_p, e_n) = (1.3e, 0.5e)$, predicts strong mixing between the sd and pf shells at ^{29}Na ($N = 18$), while ^{28}Na

is predicted to have a nearly pure 0p-0h normal *sd* configuration, and ^{30}Na a nearly pure 2p-2h intruder *pf* configuration. The $f_{7/2}p_{3/2}$ wave-function admixtures imply that significant collectivity develops for electromagnetic transitions between the low-lying positive parity states in ^{29}Na.

It is therefore of paramount importance to quantitatively determine shell-gap narrowing effects in ^{29}Na in order to assess the role of intruder configurations in the wave function. A measurement of the reduced transition matrix element would provide valuable insight into this problem since it is sensitive to nuclear collectivity through systematic changes in shell-gap strength. This work tests these predictions for the boundary nucleus ^{29}Na using sub-barrier Coulomb excitation to excite the 72-keV first-excited state in this nucleus and determine the $E2$ matrix element for its decay. In this article we report the first measurement of the reduced transition matrix element $\langle \frac{5}{2}_1^+ || E2 || \frac{3}{2}_{\text{gs}}^+ \rangle$ for ^{29}Na, from which the energy gap between the shells can be inferred.

FIG. 2: Particle-γ coincident, suppressed, random-subtracted γ-ray energy spectrum observed following $\sim$ 70 h of beam on target corresponding to ^{110}Pd(^{29}Na,^{29}Na*) at $E_{\text{beam}} =$ 70 MeV. The prominent peaks are marked and correspond to the $5/2_1^+ \rightarrow 3/2_{\text{gs}}^+$ transition at 72 keV in ^{29}Na, and the $2_1^+ \rightarrow 0_{\text{gs}}^+$ at 374 keV in ^{110}Pd.

II. EXPERIMENT

The energetic beam of ^{29}Na was obtained as follows. The radioactive ^{29}Na atoms were initially produced by fragmentation in a Ta primary target bombarded by a 500-MeV proton beam, delivered by the TRIUMF cyclotron with an intensity of 70 μA. The ^{29}Na atoms effusing out of the target were ionized to singly-charged ^{29}Na$^+$ ions in a Re surface-ion source, separated according to A/q in a magnetic sector field, and steered toward the room-temperature LINAC, ISAC-I [23], with an RFQ-injection energy of $2 \cdot A$ keV and accelerated to $150 \cdot A$ keV. The delivery of a high-quality radioactive ^{29}Na$^+$ was permitted through tuning efforts with a stable ^{58}Ni^{2+} beam. The ^{29}Na$^+$ ions were subsequently stripped to ^{29}Na^{5+} ions ($A/q = 5.8$) and post accelerated to $1.53 \cdot A$ MeV by the room-temperature Drift Tube LINAC, ISAC-I. Surviving ions were then transported to the superconducting LINAC components of ISAC-II [23, 24] via an achromatic S-bend transfer line, accelerated to a final bombarding energy of $2.41 \cdot A$ MeV (i.e. total beam energy of 70 MeV), and delivered to a secondary Coulomb-excitation target comprising a 2.94 mg/cm^2 foil of ^{110}Pd (97.6 % purity). The beam intensity on the ^{110}Pd target was as large as 600 ions/s. Six Compton-suppressed clover-segmented HPGe detectors of the TIGRESS array [25] were arranged around the target chamber. Each clover comprises 32-fold segmented HPGe detectors coupled with 12-fold segmented modular Compton suppression shields, giving rise to a total granularity of 192 discrete HPGe elements and 72 suppression elements; the TIGRESS 8-fold front-shield BGO plates were not mounted in this experiment. The front of the clover detectors was 11 cm from the target while these detectors subtended a polar laboratory range from 22.5° to 157.5°, covering approximately 36 % of the full solid angle. This arrangement is depicted in Fig. 1.
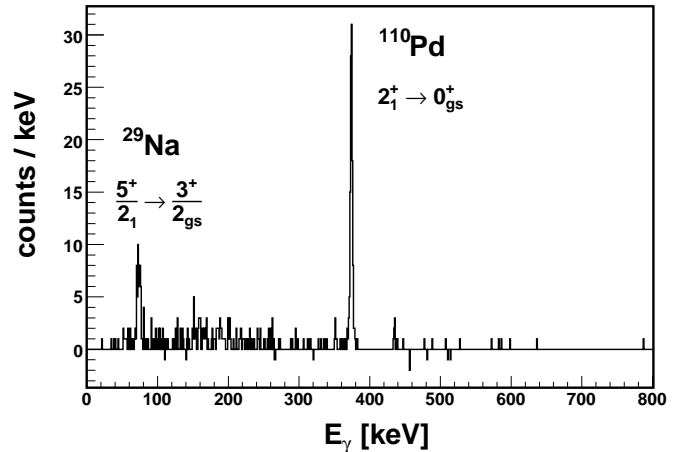
A double-sided 140-μm thick silicon detector, BAMBINO, was mounted 3 cm downstream of the target position, perpendicular to the beam direction, and was used for detection of the scattered beam and recoiling target particles. The front face of BAMBINO is segmented into 32 sector strips, while the back face is composed of 24 annular strips. This detector covered a range of forward laboratory angles between 20.1° and 49.4°. The $A = 29$ beam was dumped in a beam-stopper $\sim$ 1 m downstream of the Coulomb-excitation target. Spectra from a cylindrical 80 % HPGe detector at this position only revealed γ-decay lines belonging to the subsequent β^--decay products of ^{29}Na ($T_{\frac{1}{2}} = 44.9(12)$ ms): ^{29}Mg, ^{29}Al, and ^{29}Si.

III. RESULTS

Although it is possible to kinematically distinguish the projectile- and target-like particles through their energy as a function of the laboratory angle, in order to maximize statistics from this low event-rate experiment, the coincidence γ-ray energy spectrum presented in Fig. 2 was generated according to acceptance of either particle type impinging onto BAMBINO and thus corresponds to acceptance of both particle types arriving within the prompt-coincident event window. Inspection of the particle-γ time difference spectrum shown in Fig. 3 showed that a wide prompt particle-γ coincidence window of $\sim$ 700 ns was required in order to ensure that all low-energy ^{29}Na events were accounted for with full efficiency.

Isobaric contamination of the incident beam is often a prevalent issue and must be investigated thoroughly in radioactive-beam experiments. The particle-energy spectrum shown in Fig. 4 corresponds to the total energy
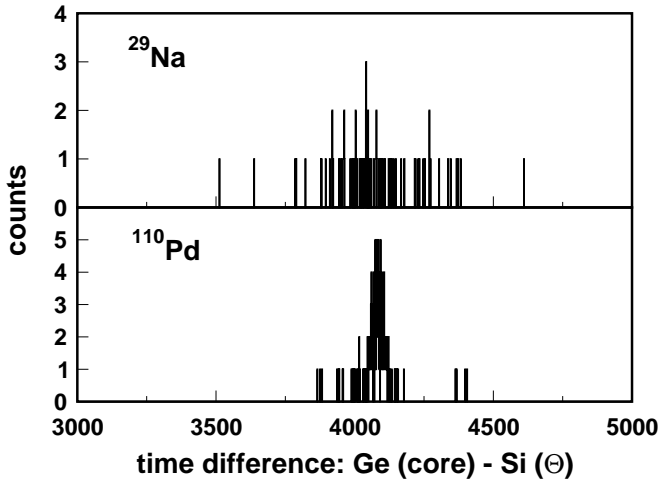
FIG. 3: Coincident timing spectra illustrating the time difference between γ and particle events. The upper panel illustrates the energy-gated time difference spectrum corresponding to ^{29}Na-like coincidence γ rays, with an energy between $E_\gamma = 66 - 78$ keV ensuring complete collection of all Doppler-shifted 72-keV γ rays over the maximum permissible range. Similarly, the lower panel shows the energy-gated time difference spectrum corresponding to ^{110}Pd-like coincident events with an energy gate from $E_\gamma = 364 - 384$ keV. The x-axis is in channel numbers [Ch] with a time-calibration constant of $10/16$ ns/Ch.

deposited in the two innermost rings of BAMBINO (covering an angular range from $20.1°$ to $23.4°$) and reveals two sharp peaks centered around 45 MeV and 50 MeV indicating a two-component beam mixture. With energy loss considerations (both in the ^{110}Pd target as well as the 0.58-mg/cm^2 thick ^{197}Au coating on the silicon strips) particle-energy peaks at 45 MeV and 50 MeV were assigned to scattered particles corresponding to ^{29}Al and ^{29}Na, respectively. The ^{110}Pd-target recoils can be identified by the broad peak at low energy in the spectrum. The $A = 29$ beam was by composition $72.0(8)$ % ^{29}Na and $28.0(8)$ % ^{29}Al, determined from this energy spectrum and the calculated Rutherford cross sections integrated over the energy losses of the isobars in the target and the total polar range subtended by the two annular strips.

Excitation of both projectile and target was observed in this experiment due to the electromagnetic interaction between the colliding nuclei. Since the average projectile-target surface distance was always greater than 5 fm at the incident bombarding energy, any nuclear interference is therefore considered negligible [26]. Under these conditions, only the lowest-lying excited state is expected to be strongly populated in each nucleus, with excitations to higher states significantly weaker, ~ 1 % or less. Determination of the transition matrix element $\langle \frac{5}{2}^+_1 || E2 || \frac{3}{2}^+_{gs} \rangle$ for ^{29}Na was accomplished according to the relative γ-ray yield between ^{110}Pd and ^{29}Na. Similar approaches have been successfully adopted in other radioactive-ion beam

Coulomb-excitation experiments that have also used the isotope separator online technique, e.g. see Ref. [16, 27–29]. The integrated γ-ray yield for the $2^+_1 \rightarrow 0^+_{gs}$ transition in ^{110}Pd was calculated directly using the multiple Coulomb-excitation code GOSIA [30] together with known properties of ^{110}Pd. The calculation was performed based on known matrix elements for all significant couplings up to the second excited 4^+ state in ^{110}Pd [31], then integrating over the energy loss of the beam through the target and over the solid angle subtended by BAMBINO corresponding to acceptance of both scattered-beam ($20.1° - 49.4°$) and recoiling-target ($20.1° - 31.0°$) particles. Corrections for angular distribution effects and internal conversion processes were also taken into account. The total observed number of ^{110}Pd γ rays had two components due to incident-beam isobaric contamination; these were derived according to excitations based on ^{29}Na/^{110}Pd and ^{29}Al/^{110}Pd monopole/quadrupole interactions. The corrected number of counts for this $2^+_1 \rightarrow 0^+_{gs}$ transition in ^{110}Pd was $90(9)$ for the ^{29}Na/^{110}Pd component, while the number of counts recorded for the $5/2^+_1 \rightarrow 3/2^+_{gs}$ transition in ^{29}Na was $56(7)$. An experimental Coulomb-excitation cross section for the $5/2^+_1 \rightarrow 3/2^+_{gs}$ transition in ^{29}Na was then deduced relative to the known $2^+_1 \rightarrow 0^+_{gs}$ transition in ^{110}Pd. The unknown ^{29}Na reduced transition matrix element $\langle \frac{5}{2}^+_1 || E2 || \frac{3}{2}^+_{gs} \rangle$ could then be treated as a variable parameter in the GOSIA calculations, while the reduced diagonal matrix element, $\langle \frac{3}{2}^+_{gs} || E2 || \frac{3}{2}^+_{gs} \rangle = 0.121(4)$ eb, was derived from a previous measurement of the ground-state quadrupole moment [17]. Effects from virtual excitation to higher-lying states in ^{29}Na were included but found to have negligible impact on the $5/2^+_1 \rightarrow 3/2^+_{gs}$ yield. The yield was also found to be insensitive to sign differences from higher-order couplings, in particular the sign of the diagonal element, $\langle \frac{5}{2}^+_1 || E2 || \frac{5}{2}^+_1 \rangle$, assumed to be $|0.026(1)|$ eb in accordance with a rotational model calculation, only leading to a yield difference at the ~ 0.1 % level depending on constructive or destructive interference modes. Systematics imply that the $5/2^+_1 \rightarrow 3/2^+_{gs}$ transition proceeds largely via an $M1$ decay mode. The estimated $|\langle \frac{5}{2}^+_1 || M1 || \frac{3}{2}^+_{gs} \rangle|$ value of 0.207 μ_N in ^{29}Na was based on previous lifetime measurements in ^{25}Na [32]. The calculated integrated γ-ray yield for the $5/2^+_1 \rightarrow 3/2^+_{gs}$ transition was found to be almost entirely insensitive to the sign and magnitude of the $M1$ matrix element, while a small yield difference of 1.5 % resulted from the angular distribution correction.

An experimental value of $|\langle \frac{5}{2}^+_1 || E2 || \frac{3}{2}^+_{gs} \rangle| = 0.237(21)$ eb has been extracted for ^{29}Na in this work, corresponding to a $B(E2; 3/2^+_{gs} \rightarrow 5/2^+_1) = 140(25)$ e^2fm^4 ($17.7(32)$ W.u. for the corresponding downward transition). These results are summarised in Tab. I alongside the theoretical predictions based on the large-scale shell-model calculations of Ref. [21]. The statistical uncertainty arising from the measured
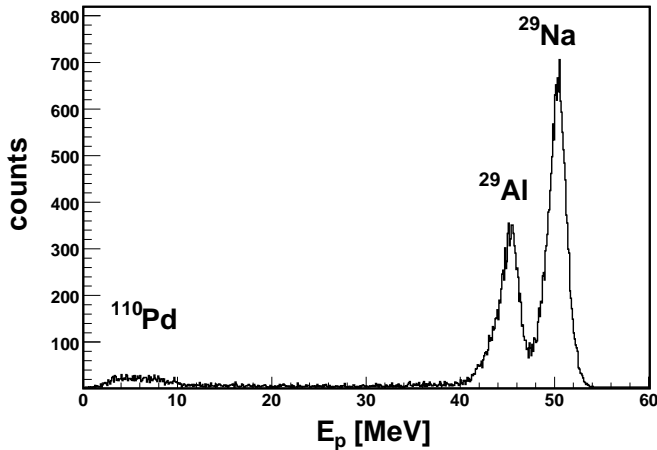
FIG. 4: Particle-energy spectrum corresponding to the total energy deposited in the two innermost annular strips of the BAMBINO silicon array. At high energy the ^{29}Al and ^{29}Na ions can be clearly separated, while the ^{110}Pd ions recoil at much lower energy. The positions of the different particle types are labeled on the spectrum. A linear energy transformation has been applied to the all events registered in the second ring to ensure the centroids corresponding to the different beam particles overlap upon summation.

peak areas, ~ 16 %, dominates the quoted 1-σ error on this measurement. Other contributions include uncertainties in the beam composition and target purity, ~ 3 % and < 0.1% respectively, along with a ~ 6 % systematic uncertainty in the magnitudes (and signs) of the matrix elements corresponding to couplings with higher-lying states in ^{110}Pd (and ^{29}Na), in addition to the ~ 2 % uncertainty on the relative γ-ray efficiency measurements; all of which are much less significant. As a consistency check cross sections for the $5/2_1^+ \rightarrow 3/2_{\text{gs}}^+$ transition in ^{29}Na were also deduced from γ-ray spectra kinematically constrained to events in coincidence with: (i) forward-scattered projectiles (^{29}Na or ^{29}Al); (ii) forward-scattered recoils (^{110}Pd). Experimental cross sections of 155(30) and 61(22) mb were attained for projectile-constrained and recoil-constrained events, respectively. These results are in good agreement with the calculated yield assuming the average value of the above reduced matrix element $\langle \frac{5}{2}_1^+ ||E2|| \frac{3}{2}_{\text{gs}}^+ \rangle$ determined in this measurement: 144 mb for projectile-constrained and 65 mb for recoil-constrained events.

TABLE I: Experimental $|\langle \frac{5}{2}_1^+ ||E2|| \frac{3}{2}_{\text{gs}}^+ \rangle|$ [eb] and $B(E2; 3/2_{\text{gs}}^+ \rightarrow 5/2_1^+)$ [e^2fm^4] values for ^{29}Na deduced in this work in comparison with theoretical predictions based on the shell-model calculations of Ref. [21].

	EXPT	SDPF-M	USD
$|\langle \frac{5}{2}_1^+ ||E2|| \frac{3}{2}_{\text{gs}}^+ \rangle|$	0.237(21)	0.232	0.211
$B(E2; 3/2_{\text{gs}}^+ \rightarrow 5/2_1^+)$	140(25)	135	111

IV. DISCUSSION

This experimental result, $|\langle \frac{5}{2}_1^+ ||E2|| \frac{3}{2}_{\text{gs}}^+ \rangle| = 0.237(21)$ eb, is consistent with the prediction of the MCSM using the SDPF-M interaction [21], $|\langle \frac{5}{2}_1^+ ||E2|| \frac{3}{2}_{\text{gs}}^+ \rangle| = 0.232$ eb, which also predicts the correct ground-state spin $I = 3/2^+$ [4] for ^{29}Na (c.f. the result using the USD interaction with $(e_p, e_n) = (1.3e, 0.5e)$: $I_{\text{gs}} = 5/2^+$; $|\langle \frac{3}{2}_1^+ ||E2|| \frac{5}{2}_{\text{gs}}^+ \rangle| = 0.211$ eb). This result therefore supports the theoretical conjecture allowing for neutron excitations across the shell gap, resulting in neutrons filling the next major pf shell before completion of the $N = 20$ sd major shell, and a strongly-mixed state comprising a $30 \sim 40$ % admixture of 2p-2h configurations in the wave function [33]. This scenario would imply a narrow sd-pf neutron-shell gap of ~ 3 MeV [21] for ^{29}Na in the ground state. The theoretical predictions describing the low-lying level structure for ^{29}Na, including the wave-function parentages of the SDPF-M prediction [33], are summarised in Fig. 5 and presented in comparison to the experimentally observed level scheme for this nucleus.

Since a successful description of the electromagnetic properties of the $5/2_1^+$ and $3/2_{\text{gs}}^+$ states in ^{29}Na assumes a similar underlying single-particle configuration, it is relevant to discuss the rotational correlations of the significantly enhanced transition probability between these two states. Within the framework of a rotational model calculation and assuming a prolate deformation, an intrinsic quadrupole moment, $Q_t = 0.524(46)$ eb, is deduced from the transition matrix element derived for ^{29}Na from this measurement. This value is in good agreement with the SDPF-M calculation, $Q_t = 0.513$ eb [21]. Contrasting behavior in the static and dynamic-nuclear properties of ^{29}Na, arising from differences in the underlying single-particle configurations of the ground and excited states, may explain the difference between the present measurement and that of an earlier experimental result using β-NMR spectroscopy, $Q_0 = 0.430(15)$ eb [17]. This intrinsic quadrupole moment, derived from the ground-state spectroscopic quadrupole moment, 0.086(3) eb, also compares well with the SDPF-M calculation, $Q_0 = 0.455$ eb.

V. SUMMARY

In the first in-beam γ-ray spectroscopy measurement using TIGRESS at the recently commissioned ISAC-II facility at TRIUMF, sub-barrier Coulomb-excitation of a radioactive beam of ^{29}Na ions has been successfully performed. From the measured γ-ray yields, the transition probability to the first excited state in this nucleus has been determined for the first time. The extracted result shows strong evidence for sd-pf shell mixing in both the ground and first-excited states in ^{29}Na, in good agreement with the SDPF-M prediction [21]. The inadequacy
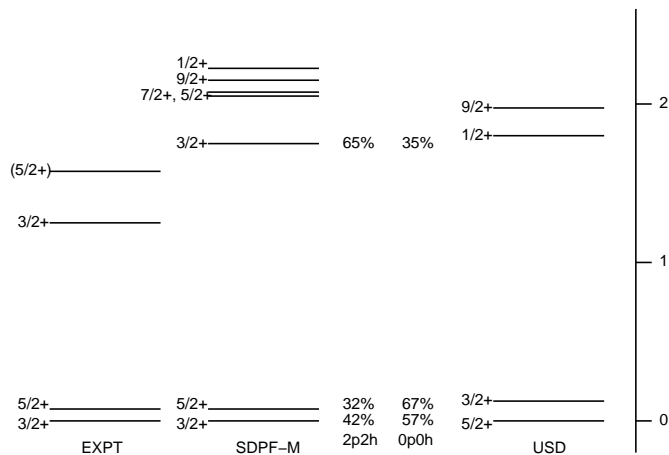
FIG. 5: Experimental energy levels for ^{29}Na shown in comparison to theoretical predictions using the SDPF-M and USD interactions. The wave-function parentages, taken from Ref. [33], refer to the SDPF-M predictions. The energy scale on the right-hand side is shown in units of MeV.

of the USD description of the ground-state properties of ^{29}Na had already been previously established from the earlier static quadrupole moment measurement [17]. This work provides further evidence in support of this scenario from a dynamic measurement of the transition probability to the first excited state in ^{29}Na. While the

main part of the island of inversion has been largely explained by theoretical interpretation, the boundary regions remain especially challenging. In the future we will extend our measurements to neighbouring nuclei ^{30}Na and ^{31}Mg in order to further test the predictive capabilities of current shell-model theories. This experiment has demonstrated the ability to perform very successful low-energy ISOL experiments with beam rates as low as only a few hundred particles per second. With the proposed advances for the next generation of γ-ray spectrometers, e.g. AGATA [34] and GRETA [35], an order of magnitude increase in γ-ray detection efficiency will be available, allowing for unparalleled access to the most exotic nuclei with beam rates as low as a few tens per second.

[1] R. Klapisch et al., Phys. Rev. Lett. **23**, 652 (1969).
[2] C. Thibault et al., Phys. Rev. C **12**, 644 (1975).
[3] X. Campi, H. Flocard, A. K. Kerman, and S. Koonin, Nucl. Phys. **A251**, 193 (1975).
[4] G. Huber et al., Phys. Rev. C **18**, 2342 (1978).
[5] C. Détraz et al., Nucl. Phys. **A394**, 378 (1983).
[6] C. Détraz et al., Phys. Rev. C **19**, 164 (1979).
[7] B. H. Wildenthal and W. Chung, Phys. Rev. C **22**, 2260 (1980).
[8] A. Watt, R. P. Singhal, M. H. Storm, and R. R. Whitehead, J. Phys. G **7**, L145 (1981).
[9] B. H. Wildenthal, Prog. Part. Nucl. Phys. **11**, 5 (1984).
[10] E. K. Warburton, J. A. Becker, and B. A. Brown, Phys. Rev. C **41**, 1147 (1990).
[11] T. Otsuka et al., Phys. Rev. Lett. **87**, 082502 (2001); T. Otsuka et al., Eur. Phys. J. A **15**, 151 (2002).
[12] Y. Utsuno, T. Otsuka, T. Mizusaki, and M. Honma, Phys. Rev C **60**, 054315 (1999).
[13] B. V. Pritychenko et al., Phys. Lett. B **461**, 322 (1999).
[14] B. V. Pritychenko et al., Phys. Rev. C **66**, 024325 (2002); S. Ettenauer et al., Phys. Rev. C **78**, 017302 (2008).
[15] G. Neyens et al., Phys. Rev. Lett. **94**, 022501 (2005).
[16] O. Niedermaier et al., Phys. Rev. Lett. **94**, 172501 (2005).
[17] M. Keim et al., Eur. Phys. J. A **8**, 31 (2000).
[18] V. Tripathi et al., Phys. Rev. Lett. **94**, 162501 (2005).
[19] V. Tripathi et al., Phys. Rev. C **73**, 054303 (2006).
[20] B. H. Wildenthal, M. S. Curtin, and B. A. Brown, Phys. Rev. C **28**, 1343 (1983).
[21] Y. Utsuno et al., Phys. Rev. C **70**, 044307 (2004).
[22] B. A. Brown, Prog. Part. Nucl. Phys. **47**, 517 (2001).
[23] R. E. Laxdal, Nucl. Instrum. Methods Phys. Res., Sect. B **204**, 400 (2003).
[24] R. E. Laxdal et al., Proc. EPAC2006, Edinburgh, Scotland (2006).
[25] H. C. Scraggs et al., Nucl. Instrum. Methods Phys. Res., Sect. A **543**, 431 (2005).
[26] D. Cline, Ann. Rev. Nucl. Part. Sci. **36**, 683 (1986).
[27] A. M. Hurst et al., Phys. Rev. Lett. 98 (2007) 072501.
[28] I. Stefanescu et al., Phys. Rev. Lett. 98 (2007) 122701.
[29] J. Cederkäll et al., Phys. Rev. Lett. 98 (2007) 172501.
[30] T. Czosnyka, D. Cline, and C. Y. Wu, Bull. Am. Phys. Soc. **28**, 745 (1983).
[31] L. Hasselgren and D. Cline, "Interacting Bose-Fermi Systems in Nuclei", Ed. F. Iachello, Plenum Press, Ettore Majorana International Science Series **10**, 59 (1980).
[32] R. L. Kozub et al., Nucl. Phys. **A403**, 155 (1983).
[33] V. Tripathi et al., Phys. Rev. C **76**, 021301(R) (2007).
[34] J. Simpson, J. Phys. G: Nucl. Part. Phys. **31**, S1801 (2005).
[35] I. Y. Lee, AIP Conf. Proc. **656**, 343 (2003).